IEEE Access
Multidisciplinary | Rapid Review | Open Access Journal

Received May 9, 2021, accepted May 31, 2021, date of publication June 7, 2021, date of current version June 14, 2021.

Digital Object Identifier 10.1109/ACCESS.2021.3086885

Epilepsy SEEG Data Classification Based On Domain Adversarial Learning

HAO YU AND MENGQI HU
Shanghai Key Laboratory of Trustworthy Computing, East China Normal University, Shanghai 200062, China
Corresponding author: Hao Yu (haoyu@stu.ecnu.edu.cn)

ABSTRACT Epilepsy is a neurological disorder characterized by recurrent epileptic seizures. Although an increasingly intense research effort has focused on the use of brain signal data to predict or detect epileptic seizures as early as possible, this problem is still computationally challenging. The main challenge is that the patient's brain signal has strong individual characteristics, and the classification model is easily disturbed by this, which may lead to false predictions, affecting the reliability of the model. Based on the development of brain signal acquisition technology and deep learning, we propose a new type of deep learning model called the *Epilepsy Domain Adversarial Neural Network* (EDANN) model, which is used to classify epileptic pre-ictal signals. EDANN integrates multiple deep neural networks based on the idea of adversarial learning, which can reduce the impact of the differences between patients on model prediction. The multi-network design in EDANN effectively improves the model training stability and model generalizability. In addition, a unique brain signal processing algorithm is developed to convert signals to data blocks that are ready for pre-ictal classification, and the model may provide an auxiliary diagnosis for early warning of epilepsy. Experimental results on real patient data show that EDANN clearly improved the F1 score by approximately 7.2% compared with the existing models. On a real dataset, our model achieved state-of-the-art results.

INDEX TERMS Brain signals, epilepsy, deep learning, domain adversarial neural network, SEEG.

I. INTRODUCTION

Epilepsy is one of the most common neurological disorders with significant social and economic impact [1] and has various underlying causes [2]. Epileptic seizure, a result of excessive and abnormal neuronal activity in the cortex of the brain, can be confirmed by scalp electroencephalogram (EEG) [3], electrocorticography (ECoG) [4], or stereo-electroencephalography (SEEG) [5].

In the recent decades, researchers have become increasingly interested in utilizing brain signal data, mostly scalp EEG, for seizure prediction or early detection [6]–[8].

This effort is motivated by the critical need to provide patients and clinicians with a reliable warning during the time between the start of measurable ictal evolution in brain signals and the onset of disabling symptoms for the patient for timely intervention and to potentially alter seizure evolution [6]. This research may also provide insights into the understanding of the underlying mechanisms of seizure initiation and propagation [8].

The associate editor coordinating the review of this manuscript and approving it for publication was Nuno Garcia.

Despite decades of progress in the development of devices and algorithms, reliable seizure prediction or early detection is still computationally challenging. First, while scalp EEG recordings have been widely used in daily practice, they are highly susceptible to various bioelectric noise sources, posing significant challenges in the analysis and interpretation of brain activities [9]. SEEG is a long-established technique for the direct capture of electrophysiological signals from the brain and records electrical activities with significantly more information and less noise than scalp EEG. However, the patient-to-patient variance of the SEEG signals may be large because that SEEG electrodes are implanted based on the potential epileptogenic zone, which varies among the patients. The high patient-to-patient variance also arises from the wide demographic distribution and various epilepsy types of the patients. Second, how early a seizure can be detected remains an open question. There is no standard definition of the duration of the pre-ictal and inter-ictal periods, although a trained neurologist can identify pre-ictal spikes 30-60 minutes prior to seizure onset [10]. The determination of the time window depends on the ability to perceive the changes in the brain signals and on the region of the seizure onset. Third, compared to the scale of the EEG datasets, which can include

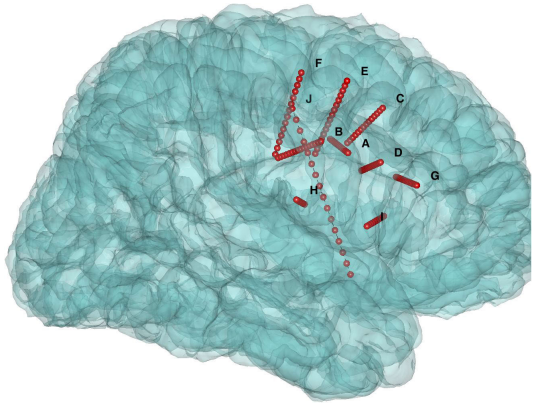

FIGURE 1. SEEG electrode locations for a patient.

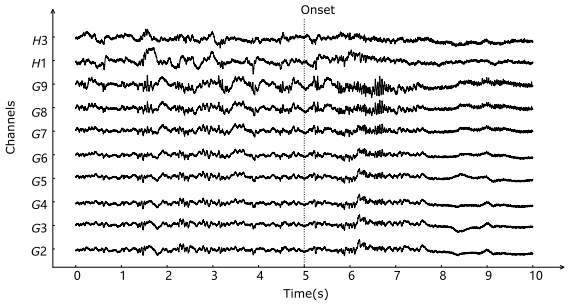

FIGURE 2. Raw SEEG data with time on the x-axis and channel name on the y-axis, where the dotted line indicates seizure onset.

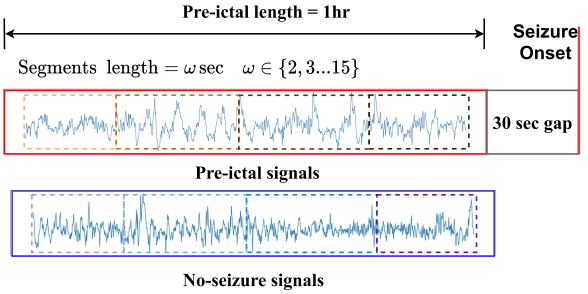

FIGURE 3. SEEG data segmentation where data for both pre-ictal signals (red) and no-seizure (blue) can be separated into 2-15 second segments.

as many as hundreds of patients in a single study [11], a limited number of patients have undergone the SEEG procedure and have had their seizures recorded. It is difficult to mobilize the existing SEEG-based analysis for epileptic pre-ictal signal classification [12], [13].

SEEG is a long-established technique to directly capture electrophysiological signals from the brain through deep electrodes surgically implanted into brain tissue [5]. It can record electrical activities with significantly more information and less noise than scalp EEG. Fig. 1 shows a 3D schematic diagram of a 27-year-old male epilepsy patient (Patient-1 of the paper). The patient has a 15-year history of seizures. To detect the epilepsy lesion, the doctor places some electrodes in the suspicious area. An SEEG electrode (e.g., A-J in Fig. 1) inserted into the human brain usually contains multiple recording contacts (typically 8-16 contacts with a 3.5 mm center-to-center distance) along each electrode's shaft. SEEG signal recordings have high amplitudes (50-1500μv) and produce changes across a wide range of frequencies (up to 10kHz) [14]. Fig. 2 shows the brain signals collected by some electrodes. According to Fig. 2, the patient has a seizure at approximately 5 seconds. Leveraging high-quality SEEG data and recent advances in deep learning, we propose a novel deep learning algorithm called *Epilepsy Domain Adversarial Neural Network (EDANN)* that can distinguish seizures from non-seizure using SEEG signals a certain time prior to seizure onset (see Fig. 3). SEEG can record electrical activities with significantly more information and less noise than scalp EEG. In this paper, we consider all SEEG data from the same person to have the same domain. Because these data often have the same individual characteristics, this domain information will mislead the classifier, resulting in weak model generalization ability. The EDANN model is designed based on the idea of adversarial learning. It is mainly composed of three parts, encoder, domain discriminator, and label classifier. The encoder is responsible for dimensionality reduction and local feature extraction. The domain discriminator guides the encoder to remove the domain information, and the label classifier completes the classification on this basis. In the process of mutual adversarial learning, the model can finally complete the classification task without being affected by domain information, greatly enhancing the generalization ability of the model. The Python-based code can be found here.[1]

The main contributions of our work can be summarized as follows:

- To the best of our knowledge, this study is the first to conduct more systematic mining of SEEG epilepsy signals using the deep learning method.
- This paper proposes a deep learning model based on epilepsy domain adversarial learning, which can adaptively classify different SEEG signals and achieves state-of-the-art results compared with the benchmark model on a real dataset. Our model may be used in actual epilepsy diagnosis in the future.
- We constructed a real epilepsy SEEG dataset and verified the effectiveness of our model.

II. RELATED WORK

In recent years, tools have been developed to characterize seizure patterns from brain signals. However, most of the tools are focused on scalp EEG data. Boashash *et al.* [15] extracted seizure characteristics from newborn EEG by representing the EEG signals in the time-frequency domain using the Beta distribution. Schiff *et al.* [16] developed a modern numerical approach based on singular value decomposition that can be applied to search for dynamically distinct stages of

[1]https://github.com/danzhewuju/Epilepsy-Domain-Adversarial-Neural-Network

epileptic seizures in humans. Dorr *et al.* [17] identified similarities in the spatio-temporal dynamics of epileptic seizures based on EEG. The method determined the time-varying degree of nonlinear correlations between the scalp electrodes at the seizure onset and during seizure spread. Fan *et al.* [18] developed a multivariate seizure detection approach by representing the EEG signals with a recurrence network.

Deep neural networks have been increasingly used for EEG signal analysis. Yao *et al.* [19] identified epileptic seizures through the analysis of EEG data, and this method later became the standard machine learning approach for identifying seizures from EEG data. Abramovici *et al.* [20] assessed the utility of simultaneous scalp EEG in patients with focal epilepsy undergoing intracranial EEG evaluation after detailed presurgical testing. Chang *et al.* [21] found that the transition from normal to seizure is not a sudden phenomenon. Instead, it is a slow process that can be characterized by the progressive loss of neuronal network resilience. Truong *et al.* [22] applied a CNN-based generalized retrospective and patient-specific seizure classification model using intracranial and scalp EEG data.

Although the existing works have revealed the EEG seizure patterns in great detail, they cannot be directly adopted to analyze SEEG data, mainly because: 1) the EEG channel position is relatively fixed, whereas the SEEG electrodes are implanted based on detailed analysis of an anato-electro-clinical study of the potential epileptogenic zone of every patient; 2) the sampling frequency of EEG is much lower than that of SEEG; and 3) manual parameter adjustment is still inevitable when applying a trained model to new patients. To date, only a few studies have attempted to identify seizure patterns in SEEG data. Brainstorm [12] is a collaborative application with a rich and intuitive graphic interface dedicated to the analysis of brain recordings, including EEG, ECoG, and SEEG. MNE [13] is a tool for exploring, visualizing, and analyzing neurophysiological data. Sharma *et al.* [23] developed a tool to predict seizure timing and identify epileptic areas from SEEG data. Zhang *et al.* [24] developed an epileptic seizure classification tool to analyze the power spectrum of the SEEG signals. However, the applicability of these tools remains limited due to the high data complexity.

III. METHOD

We propose EDANN for epileptic pre-ictal signal classification, which will be beneficial for research on epilepsy early warning.

A. SEEG DATA PREPROCESSING

We expect the model to capture the SEEG features between multiple channels in the data preprocessing stage and then learn the global SEEG features. First, the channels of the SEEG signal can be reordered, and the formal expression is as follows: Let $C = \{c_1, c_2, c_3 \ldots c_n\}$ represent the set of physical coordinates of all n channels in the SEEG signal. Here $c_i (i = 1 \ldots N)$ represents the physical coordinates of the ith channel in C. We can define an undirected complete graph $G(V, E)$, where V represents a collection of channel nodes. v_i denotes the ith node in V, and its corresponding physical coordinate is c_i. E represents the set of edges, and $e_{i,j}$ represents the edges that exist between nodes v_i and v_j. For the edges, the weight value on any edge $e_{i,j}$ is defined as follows:

$$w\left(e_{i,j}\right) = D\left(v_i, v_j\right) \tag{1}$$

where $D(\cdot)$ represents the Euclidean distance. In $G(V, E)$, there is a subset of T in E. The minimum spanning tree can be constructed by minimizing the global weight value. $W(T)$ is expressed as the sum of the weights of the edges of the minimum spanning tree. The formal expression is as follows:

$$\mathrm{W}(T) = \min\left(\sum_{e_{i,j} \in T} w\left(e_{i,j}\right)\right) \tag{2}$$

The overall flow chart is shown in Fig. 4. Fig. 4(a) shows the distribution of channel contacts in the brain space; Fig. 4(b) shows a deep search at any node in the constructed minimum spanning tree; Fig. 4(c) is completed through a deep search; and Fig. 4(d) shows that the original SEEG signals are reordered according to the sequence. From Fig. 4(d), it is observed that there is a certain similarity between the SEEG signals of adjacent channels, which helps the model better encode SEEG signal features. On the one hand, adjacent channels have similar SEEG signals, and arranging similar SEEG signals can make it easier for the model to learn local features. On the other hand, this method can realize personalized data preprocessing. The number and location of each person's channels are inconsistent. Through the data preprocessing method, different sequences can be generated for different people, providing more effective use of the information contained in the SEEG data. Finally, due to the long recording time of the SEEG data, the data are not easy to process and analyze, so this article adopts a standard processing method to slice the SEEG signal. The original SEEG signal is represented as a matrix, where the abscissa of the matrix represents time, and the ordinate represents the sorted channel sequence, as shown in Fig. 4(d). Next, the SEEG signal must be sliced, and the related processing procedure can be formally expressed as follows:

$$X = win(flt(sampl(Z, r), f_{low}, f_{high}), \omega) \tag{3}$$

where $sampl(.)$ is a resampling function with sampling rate r, $flt(.)$ is a band passing function, where f_{low} and f_{high} are the low- and high-frequency thresholds, and $win(.)$ is a window function for converting a long SEEG signal into variable-length segments, with its length being ω, where ω is not a fixed value but rather a random value within a certain range.

Overall, to approach the realistic case, we process the original data into fragments of 2-15 seconds. For the model,

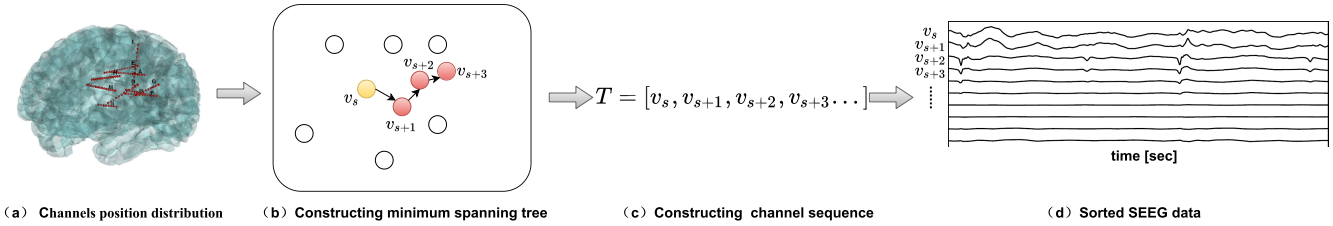

FIGURE 4. Schematic diagram of the SEEG data preprocessing.

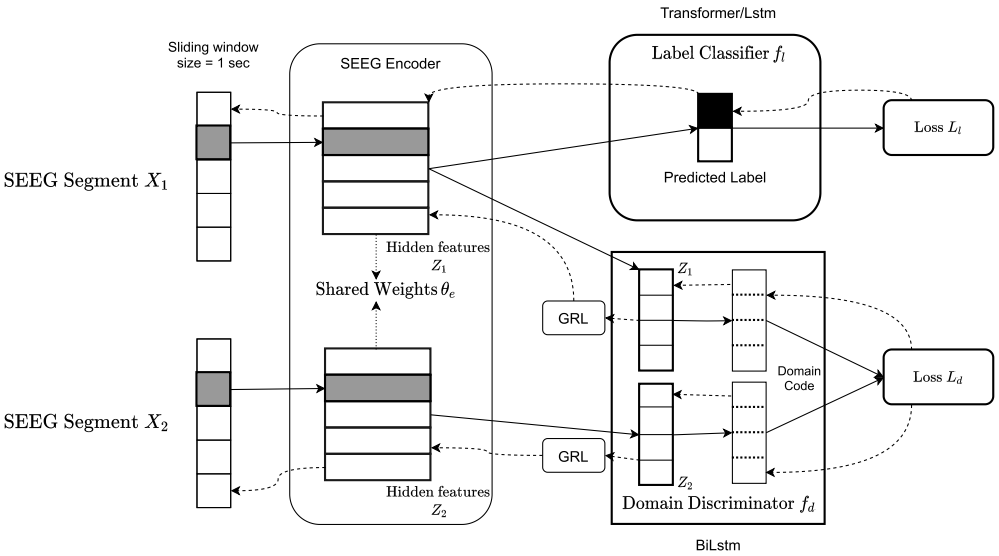

FIGURE 5. EDANN contains 3 modules. The structure of EDANN consists of an encoder, a label classifier, and a domain discriminator. The encoder is a convolutional neural network (CNN) [25], which learns an embedding for every 1 second of the SEEG segment. The label classifier is a Transformer [26] or LSTM model that is used to discriminate the target SEEG data. The domain discriminator is a bidirectional long short-term memory (BiLSTM) model [27] that determines whether a pair of data comes from the same patient. It can help the encoder reduce the difference between individuals and learn the correct characteristics.

identification of variable-length fragments is more complex than the task of identifying fixed-length fragments because the variable length of the data segment requires the model to be able to learn the critical features of the SEEG signal truly. The difference in the segment length (minimum length 2 s, maximum length 15 s) is particularly significant. The setting can help our model deal with more complex situations; these fragments will serve as input to our model. At the same time, it can also learn the possible associations between the SEEG sequences.

B. PRE-ICTAL SIGNAL CLASSIFICATION

The EDANN model includes three main modules: encoder, label classifier, and domain discriminator. Its structure is shown in Fig. 5. The encoder is mainly used to encode the original raw SEEG data and can learn the relevant EEG features from the SEEG signal and reduce the dimensionality of the data. The domain discriminator is mainly used to determine whether a pair of SEEG segments are different. For the same patient, the domain discriminator can be optimized adversarially through the gradient reversal layer (GRL) module. This ensures that the network cannot classify based on domain knowledge and reduces the interference of the SEEG data in the model due to individual differences. The class discriminator classifies the target SEEG data.

The encoder can be represented as $f_e(X; \theta_e)$ and can extract multi-channel EEG signals while reducing the dimensions of the original SEEG signals. θ_e represents the parameters of the encoder. The label classifier can be expressed as $f_l(f_e; \theta_l)$, which is an attempt to predict the label of input X, where θ_l represents the parameters learned by the discriminator. The domain discriminator can be expressed as $f_d(f_e; \theta_d)$, which aims to determine whether a pair of inputs X_1 and X_2 are from the same patient. Here, X_2 is based on random sampling. The final loss comes from two parts, where the first component is the prediction loss of the label classifier $\mathcal{L}_l(f_l(f_e; \theta_l))$ and the other component is the loss of the domain discriminator $\mathcal{L}_d(f_d(f_e; \theta_d))$. For a pair of input X_1 and X_2, the loss is given as follows:

$$\begin{aligned}&\mathcal{L}\left(X_1, X_2; \theta_e, \theta_l, \theta_d\right)\\ &\quad = \mathcal{L}_l\left(f_l\left(f_e\left(X_1; \theta_e\right); \theta_l\right)\right)\\ &\qquad -\gamma\,\mathcal{L}_d\left(f_d\left(f_e\left(X_1; \theta_e\right); \theta_d\right), f_d\left(f_e\left(X_2; \theta_e\right); \theta_d\right)\right) \quad (4)\end{aligned}$$

where γ are hyperparameters. For convenience, we use Z_1 and Z_2 to denote the hidden representations of X_1 and X_2 calculated from encoder $f_e(X;\theta_e)$. The loss of the label classifier $\mathcal{L}_l(f_l(Z_1;\theta_l))$ can be denoted with binary cross entropy:

$$\mathcal{L}_l(f_l(Z_1;\theta_l)) = -[y_1 \log f_l(Z_1) + (1-y_1)\log(1-f_l(Z_1))] \tag{5}$$

where y_1 represents the label of input data X_1, and $f_l(Z_1)$ denotes the value of the prediction by the label classifier.

The constructive loss of the domain discriminator $\mathcal{L}_d$ can be expressed as follows:

$$\begin{aligned}&\mathcal{L}_d\left(f_d\left(Z_1;\theta_d\right), f_d\left(Z_2;\theta_d\right)\right)\\ &= \frac{1}{2} D\left(f_d\left(Z_1\right), f_d\left(Z_2\right)\right)^2 I\\ &\quad + \frac{1}{2}\left(\max\left\{0, m - D\left(f_d\left(Z_1\right), f_d\left(Z_2\right)\right)\right\}\right)^2 (1-I)\end{aligned} \tag{6}$$

where I can be either 0 or 1, with $I = 1$ indicating that the two samples are from the same patient and $I = 0$ indicating the opposite. $D(.)$ is the Euclidean distance, and m is the margin that indicates the prediction boundary. The loss of all samples, $\mathcal{L}_t$, is defined as follows:

$$\mathcal{L}_t = \sum_{i,j}^{N} \alpha \mathcal{L}(X_i, X_j; \theta_e, \theta_l, \theta_d) \tag{7}$$

where N represents the number of data pairs. X_i and X_j represent the input data pair, α indicates the hyperparameters, and θ_e, θ_l and θ_d are the parameters of the encoder, label classifier and domain discriminator, respectively.

The domain classifier of the EDANN model is a BiLSTM model. The working principle of BiLSTM is to first extract the local features of the SEEG signal space of the window (window size = 1 s) through a convolutional neural network. The CNN model encodes a 16-dimensional representation of each second SEEG signal (1 s), so that the original SEEG segment can be expressed as a matrix with a matrix size of $n \times 16$, where n represents the length of the SEEG segment ($n \cdot s, n \in [2, 15]$). Then, BiLSTM is used to capture the relationship between the representations of the two directions, and then learn the global characteristics of the SEEG signal in time. According to the global characteristics, it can be judged whether two SEEG segments come from the same domain (whether two SEEG segments come from the same patient.).

EDANN's label classifier is an LSTM or Transformer model. According to the different selected models, EDANN models can be divided into EDANN-LSTM and EDANN-Transformer. The label classifier can classify the SEEG segment according to the representation learned by the encoder.

IV. EXPERIMENTAL RESULTS

A. DATASET

We collect the SEEG data from multiple epilepsy patients (an average of 130 channels per patient) from Huashan Hospital affiliated with Fudan University in Shanghai. There are a total of 24 patients' SEEG information, for which pre-ictal SEEG data (within an hour before the seizure) and no-seizure SEEG data (more than 12 hours after epileptic seizures) are collected from 5 patients, and only pre-epilepsy SEEG information is collected from 19 patients. We record many times for each patient. Limited by the incompleteness of the actual medical data, there are cases where some patient data collection is incomplete. All the information is shown in Table 1. For patients-I-V, we sample 2000 and 6000 fragments of variable length for the pre-ictal and no-seizure categories, respectively. The fragment length ranges from 2 s to 15 s. For the other patients, we use the following calculation formula to calculate the number of samples:

$$count = \frac{duration * 2 * k}{max\_window - min\_window} \tag{8}$$

where *duration* represents the total length of the record. *max_window* and *min_window* represent the maximum and minimum lengths of the SEEG segments, respectively, and k denotes the number of resampling. Equation 8 can make full use of each patient's SEEG data and can also take into account the large difference in the length of the data for each patient. The specific fragment information is presented in Table 2.

TABLE 1. SEEG dataset information.

Patient	Pre-ictal[sec]	Normal[Sec]
patient-I	4184	14398
patient-II	1412	14398
patient-III	4874	15918
patient-IV	8456	14394
patient-V	1362	14362
patient-VI	773	-
patient-VII	199	-
patient-VIII	3047	-
patient-IX	318	-
patient-X	5012	-
patient-XI	159	-
patient-XII	131	-
patient-XIII	239	-
patient-XIV	1259	-
patient-XV	311	-
patient-XVI	383	-
patient-XVII	224	-
patient-XVIII	550	-
patient-XIX	75	-
patient-XX	250	-
patient-XXI	182	-
patientXXII	74	-
patient-XXIII	36	-
patient-XXIV	33	-

TABLE 2. Number of SEEG segments.

Patient	Number of pre-ictal segments	Number of no-seizure segments
patient-I	2000	6000
patient-II	2000	6000
patient-III	2000	6000
patient-IV	2000	6000
patient-V	2000	6000
other patients	3585	0

B. EVALUATION METRIC

The evaluation measurements, including accuracy, precision, recall (sensitivity), f1 score, area under the curve (AUC) and false alarm rate (FAR), are defined as follows:

$$\text{Accuracy} = \frac{TP + TN}{TP + TN + FP + FN} \tag{9}$$

$$\text{Sensitivity} = \text{Recall} = \frac{TP}{TP + FN} \tag{10}$$

$$\text{Precision} = \frac{TP}{TP + FP} \tag{11}$$

$$F1\ \text{score} = \frac{2 \times \text{Precision} \times \text{Recall}}{\text{Precision} + \text{Recall}} \tag{12}$$

$$FAR = \frac{FP}{FP + TN} \tag{13}$$

where TP is the number of true pre-ictal (pre-seizure) SEEG segments, FN is the number of false no-seizure SEEG segments, TN is the number of true no-seizure (normal) SEEG segments, and FP is the number of false pre-ictal SEEG segments. The F1 score is often used to evaluate the performance of a model under unbalanced data, and the FAR index is often used to measure the misreporting of epilepsy by software in the diagnosis of clinical epilepsy. The definition of AUC is the area under the ROC [28] curve.

C. EXPERIMENTAL SETTING

To make the model more suitable for the actual situation, we use the leave-one-out method to verify the performance of the model. We select 5 patients who had both pre-ictal SEEG data and no-seizure SEEG data as the test set, and all of the remaining data are used as the training set. We use the traditional machine learning method based on convolutional support vector machine CNN-SVM [29] and neural network-based methods such as VDCNN [30], DPCNN [31], CNN-Voting [31], PIESD [32], LSTM [33] and Transformer [34] for comparison. We use the same data preprocessing and data input for all of the methods. In the CNN-SVM method, we learn the hidden representation of SEEG data for each window (window size = 1 s) through the CNN model and finally use the SVM model for classification. In the CNN-Voting method, the model gives a prediction result for each window (window size = 1 s) and finally gives the final prediction result through voting. VDCNN and DPCNN are commonly used for sentence classification, but if the word embedding is replaced with a window data representation (window size = 1 s), then the VDCNN and DPCNN models can also be used for classification of SEEG or EEG signals. Patient-Independent Epileptic Seizure (PIESD) is an EEG seizure classification algorithm based on adversarial learning, but PIESD is a classification algorithm with a fixed length data input. In the experiment, we use the setting reported by Zhang *et al.* to reduce the length of the input data to 1 s [32]. At the same time, we compare the experimental effects of replacing the category discriminator of the domain adversarial neural network with LSTM (EDANN-LSTM) and Transformer (EDANN-Transformer). The EDANN-Transformer and EDANN-LSTM models use the same CNN encoder structure. The encoder includes four convolutional layers, four max-pooling layers, four ReLu regularization functions and a Dropout(0.5) layer. Finally, the dimension of the hidden vector is 32. Both models use the same BiLSTM domain discriminator, which contains 2 bidirectional LSTM layers and 64 hidden units.

In the experiment, the main difference between the EDANN-Transformer (EDANN-LSTM) model and the Transformer (LSTM) model is that there is a domain discriminator. They have the same encoder module and label classifier. The label classifier Transformer of EDANN-Transformer has the same structure as that used in paper [35]. The label classifier Transformer of EDANN-LSTM includes 64 hidden units. All of the methods use the same data preprocessing. The learning rate α of EDANN-* model is set to 0.0005, and hyperparameter γ is set to 0.3. EDANN models are built on the Pytorch framework and are deployed on a server with an Intel i9 CPU and NVIDIA GeForce RTX 2080Ti. On average, 14 h are required to complete the model training.

D. EXPERIMENTAL RESULTS

Tables 3-7 show the performance of our model and the benchmark model on the SEEG data of 5 test patients. An examination of the results presented in the Tables shows that the domain-based adversarial SEEG classification method proposed in this paper achieves the best results. In particular, the method based on EDANN-Transformer achieves the best results on all patients with respect to the F1 score. Tables 4 and 5 show that our model outperforms the benchmark model by approximately 4.5% in terms of the F1 score. This is due to the nature of the SEEG signal. Because the SEEG signal has non-stationary characteristics, the epilepsy characteristics of some people are more obvious, so even a relatively simple model can perform well. According to Tables 3, 6 and 7, the EDANN-Transformer model outperforms the baseline model by approximately 9% in terms of the F1 score, which also shows that the idea of using domain adversarial learning can effectively reduce the interference of individual information. At the same time, we can also see from Tables 3-7 that the PIESD method based on adversarial learning performs similarly to the general CNN-based method. However, they are inferior to the time series model (LSTM and Transformer) in processing variable-length data.

In terms of the FAR, our models, including EDANN-LSTM and EDANN-Transformer, are generally stable with lower FAR, which is important in clinical practical applications. An examination of the data presented in Table 3 shows that our model has the worst FAR index of 2.67%, which is still a quarter of that of the best benchmark model performance. Table 5 shows that our model EDANN-Transformer has the best FAR index of 0.45%, which is also better than the benchmark model.

TABLE 3. Performance of EDANN and all of the compared methods on pre-ictal signal classification using SEEG data of patient-I.

Methods	Accuracy	Precision	Sensitivity/Recall	F1 Score	AUC	FAR
SVM	0.7902±0.0308	0.3836±0.0188	0.4258±0.0036	0.4036±0.0078	0.6445±0.0115	0.1368±0.0128
VDCNN	0.8381±0.0378	0.5081±0.0380	0.9075±0.0218	0.6515±0.0089	0.9102±0.0062	0.1756±0.0195
DPCNN	0.8812±0.0171	0.6161±0.0117	0.7625±0.0334	0.6815±0.0516	0.9290 ±0.0124	0.0950±0.0107
CNN-Voting	0.8808±0.0035	0.6823±0.0156	0.5333±0.0495	0.5986±0.0279	0.8723±0.0438	0.1496±0.0142
PIESD	0.8928±0.0126	0.6912±0.0037	0.8012±0.0189	0.7421±0.0090	0.9157±0.0085	0.0851±0.0178
LSTM	0.7381±0.0111	0.6658±0.0234	0.7433±0.0320	0.7049±0.0261	0.7903±0.0214	0.1543±0.0138
Transformer	0.7261±0.0169	0.7014±0.0294	0.6786±0.0415	0.6898±0.0129	0.8001±0.0064	0.1803±0.0174
EDANN-LSTM	0.9102±0.0103	0.7239±0.0270	0.8741±0.0253	0.7920±0.0362	0.9689±0.0011	0.0385±0.0078
EDANN-Transformer	0.9501±0.0094	0.8650±0.0170	0.8550±0.0087	0.8601±0.0491	0.9727±0.0067	0.0267±0.0009

TABLE 4. Performance of EDANN and all of the compared methods on pre-ictal signal classification using SEEG data of patient-II.

Methods	Accuracy	Precision	Sensitivity/Recall	F1 Score	AUC	FAR
SVM	0.9309±0.0173	0.7677±0.0167	0.8400±0.0152	0.8022±0.0320	0.8945±0.0165	0.0508±0.0011
VDCNN	0.8716±0.0253	0.5679±0.0144	0.9616±0.0144	0.7141±0.0019	0.9692±0.0150	0.1463±0.0137
DPCNN	0.9675±0.0215	0.8364±0.0238	0.9233±0.0418	0.8777±0.0207	0.9044±0.0118	0.0236±0.0068
CNN-Voting	0.9070±0.0118	0.6475±0.0250	0.9008±0.0302	0.7534±0.0172	0.9856±0.0199	0.1056±0.0155
PIESD	0.9423±0.0396	0.7869±0.0097	0.8045±0.0156	0.7956±0.0038	0.9445±0.0344	0.0547±0.0108
LSTM	0.9519±0.0213	0.7994±0.0126	0.9400±0.0243	0.8640±0.0248	0.9701±0.0252	0.0476±0.0076
Transformer	0.9691±0.0174	0.8844±0.0158	0.8875±0.0131	0.8656±0.0328	0.9843±0.0258	0.0545±0.0007
EDANN-LSTM	0.9793±0.0197	0.9434±0.0050	0.9316±0.0052	0.9375±0.0084	0.9905±0.0109	0.0112±0.0021
EDANN-Transformer	0.9825±0.0190	0.9423±0.0145	0.9533±0.0320	0.9478±0.0196	0.9932±0.0012	0.0117±0.0005

TABLE 5. Performance of EDANN and all of the compared methods on pre-ictal signal classification using SEEG data of patient-III.

Methods	Accuracy	Precision	Sensitivity/Recall	F1 Score	AUC	FAR
SVM	0.9015±0.0398	0.9138±0.0230	0.9016±0.0156	0.9077±0.0217	0.9815±0.0100	0.1385±0.0036
VDCNN	0.9844±0.0096	0.9755±0.0254	0.9300±0.0243	0.9522±0.0230	0.9965±0.0053	0.0046±0.0040
DPCNN	0.9634±0.0112	0.9345±0.0347	0.9645±0.0360	0.9392±0.0352	0.9698±0.0339	0.0193±0.0064
CNN-Voting	0.9772±0.0242	0.9490±0.0103	0.8633±0.0182	0.9041±0.0031	0.9987±0.0120	0.1121±0.0107
PIESD	0.9748±0.0186	0.9377±0.0120	0.9718±0.0256	0.9544±0.0156	0.9889±0.0006	0.0287±0.0078
LSTM	0.9856±0.0136	0.9315±0.0304	0.9866±0.0087	0.9583±0.0245	0.9993±0.0079	0.0145±0.0085
Transformer	0.9851±0.0200	0.9213±0.0192	0.9958±0.0012	0.9571±0.0187	0.9995±0.0054	0.0170±0.0110
EDANN-LSTM	0.9915±0.0359	0.9991±0.0301	0.9500±0.0102	0.9739±0.0120	0.9997±0.0231	0.0062±0.0067
EDANN-Transformer	0.9958±0.0240	0.9779±0.0159	0.9975±0.0301	0.9876±0.0191	0.9997±0.0085	0.0045±0.0144

TABLE 6. Performance of EDANN and all of the compared methods on pre-ictal signal classification using SEEG data of patient-IV.

Methods	Accuracy	Precision	Sensitivity/Recall	F1 Score	AUC	FAR
SVM	0.8790±0.0189	0.5846±0.0156	0.9466±0.0072	0.7228±0.0345	0.9060±0.0485	0.1345±0.0155
VDCNN	0.8787±0.0281	0.5805±0.0337	0.9816±0.0360	0.7296±0.0280	0.9832±0.0508	0.1418±0.0173
DPCNN	0.9683±0.0046	0.8844±0.0158	0.9316±0.0164	0.9074±0.0141	0.9828±0.0195	0.0243±0.0032
CNN-Voting	0.9356±0.0458	0.7270±0.0197	0.9833±0.0214	0.8359±0.0104	0.9881±0.0243	0.1738±0.0162
PIESD	0.9366±0.0261	0.8326±0.0288	0.9267±0.0190	0.8771±0.0208	0.9736±0.0253	0.1324±0.0188
LSTM	0.9273±0.0367	0.7018±0.0092	0.9808±0.0039	0.8182±0.0135	0.9905±0.0256	0.0833±0.0074
Transformer	0.9376±0.0224	0.8511±0.0056	0.9766±0.0154	0.9095±0.0266	0.9933±0.0251	0.0341±0.0011
EDANN-LSTM	0.9666±0.0050	0.8443±0.0046	0.9808±0.0051	0.9074±0.0060	0.9948±0.0177	0.0385±0.0018
EDANN-Transformer	0.9869±0.0001	0.9570±0.0281	0.9650±0.0323	0.9609±0.0111	0.9925±0.0040	0.0086±0.0024

TABLE 7. Performance of EDANN and all of the compared methods on pre-ictal signal classification using SEEG data of patient-V.

Methods	Accuracy	Precision	Sensitivity/Recall	F1 Score	AUC	FAR
SVM	0.6366±0.0466	0.3083±0.0147	0.4258±0.0220	0.3577±0.0020	0.6445±0.0212	0.1368±0.0121
VDCNN	0.7888±0.0397	0.4267±0.0131	0.7741±0.0311	0.5501±0.0275	0.8550±0.0413	0.2082±0.0228
DPCNN	0.7643±0.0156	0.4062±0.0045	0.8933±0.0367	0.5584±0.0066	0.9037±0.0197	0.2614±0.0233
CNN-Voting	0.9070±0.0142	0.7043±0.0040	0.7625±0.0128	0.7322±0.0373	0.9542±0.0370	0.0640±0.0032
PIESD	0.8245±0.0139	0.6728±0.0076	0.7289±0.0091	0.6997±0.0068	0.9347±0.0084	0.1582±0.0015
LSTM	0.7955±0.0245	0.6431±0.0082	0.7800±0.0284	0.7049±0.0152	0.9116±0.0144	0.2213±0.0213
Transformer	0.8579±0.0150	0.6477±0.0297	0.7516±0.0001	0.6958±0.0060	0.9331±0.0467	0.1408±0.0149
EDANN-LSTM	0.9364±0.0229	0.8290±0.0191	0.7800±0.0253	0.8037±0.0126	0.9711±0.0097	0.0322±0.0025
EDANN-Transformer	0.9387±0.0275	0.8570±0.0165	0.7591±0.0026	0.8051±0.0065	0.9760±0.0204	0.0253±0.0039

To verify the effect of reordering the SEEG segment rows in the data preprocessing, we use the EDANN-Transformer model to compare the performance with different channel ordering methods on five patients. In Fig. 6, Reordering means using our sorting method, and Random means using the SEEG default channel order (the SEEG default order is

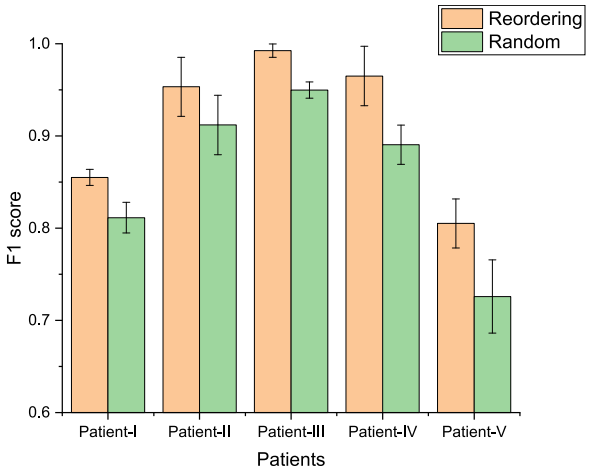

FIGURE 6. Influence of different ordering of the channels on the EDANN-Transformer model in data preprocessing.

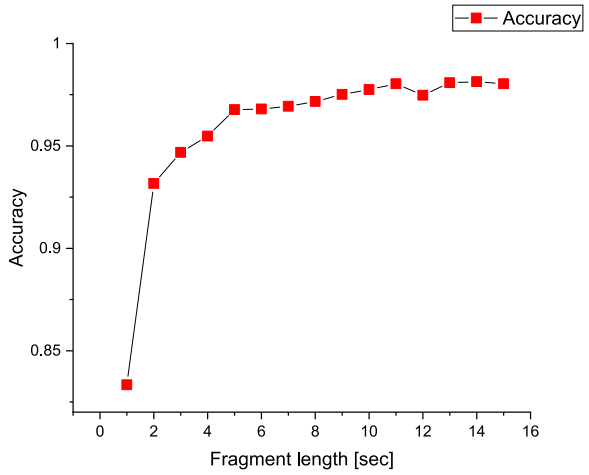

FIGURE 7. Impact of fragment length on accuracy.

sorted according to the channel ID). Experimental results show that the performance of EDANN-Transformer on the data after channel reordering is 5.33% better than the random order on average, proving the effectiveness of data preprocessing.

Since our model uses variable-length data for training, we compare the accuracy for data with different lengths. Fig. 7 shows how the accuracy of the model (EDANN-Transformer) varies with different sizes of the fragment length. It is observed from Fig. 7 that when the fragment length is less than 5 s, the accuracy rate increases drastically with increasing fragment length; when the fragment length size is 5-11 s, as the fragment length increases, the accuracy of the model increases slowly; and when the fragment length is longer than 11 s, as the length increases, the accuracy of the model remains basically unchanged. This shows that the model requires a specific fragment length size to capture relevant signals. The amount of information obtained by our model decreases with decreasing fragment length,

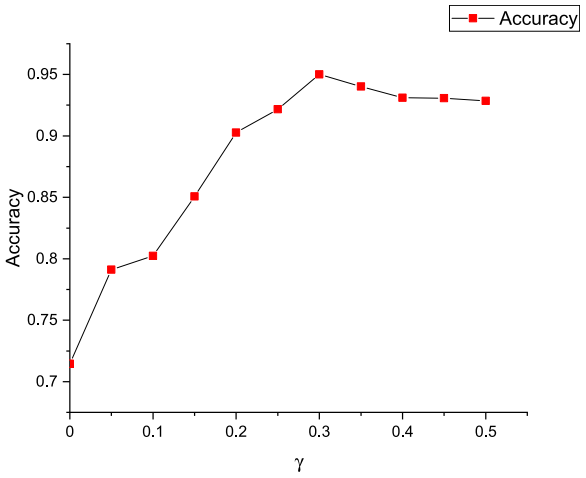

FIGURE 8. Impact of hyperparameter γ on the accuracy for patient-I SEEG data.

TABLE 8. Ablation experiment exploring the influence of the domain discriminator on the experiment.

	label classifier	F1 score
-domain discriminator	LSTM	0.7049
	Transformer	0.6898
+domain discriminator	LSTM	0.7920
	Transformer	0.8601

increasing the likelihood of wrong predictions. However, too long fragments increase the noise in the data, which will also reduce the model's prediction accuracy. The experiment shows that the optimal recognition fragment length size of the model is approximately 11 s. In the clinic, the time required by the doctors to recognize epilepsy characteristic signals is approximately ten seconds, which is consistent with our experimental results.

The parameter γ in the experiment has a significant influence on the accuracy. We explore the influence of parameter γ from 0 to 0.5 on the EDANN-Transformer model for the SEEG data of patient-I. It is observed from Fig. 8 that when γ is less than 0.3, the accuracy of the model increases with increasing γ. When $\gamma = 0.3$, the accuracy of the model reaches the maximum value of approximately 95%, and as γ increases, the accuracy of the model gradually decreases. This trend is observed because when γ is small, the contribution of the domain discriminator to the entire model is relatively small, and the model can easily learn incorrect information about the patient, leading to low performance of the model. When γ is greater than 0.3, the domain discriminator interferes with the learning of the label classifier, and the accuracy of the model decreases. This means that the domain discriminator is important for the appropriate functioning of the EDANN-* model.

To further study the influence of the domain discriminator and label classifier on the experiment, we conduct an ablation experiment, with the results shown in Table 8,

in which -domain discriminator means that the domain discriminator is removed, and +domain discriminator means to that the domain discriminator is added. We use LSTM and Transformer as the label classifier to compare their experimental F1 score results. It is observed from Table 8 that the domain discriminator has a greater impact on the F1 score of the experiment. In particular, the impact on the Transformer model is more pronounced. Probably because the model parameters of LSTM are fewer than those of the Transformer model, the domain discriminator is not as helpful to the LSTM model as it is to the Transformer model.

V. CONCLUSION

In this paper, we propose an SEEG classification algorithm based on domain adversarial learning. This method adopts the idea of adversarial learning and uses the domain discriminator to supervise the encoder to perform encoding by removing individual information, and the label classifier is used to guide the encoder to extract the SEEG features. Through the adversarial learning method, the encoder can not only learn the relevant characteristics of SEEG but also remove the interference of individual information. This algorithm shows improved performance on a real epilepsy diagnosis dataset. This has positive significance for SEEG signal processing and clinical medical treatment.

REFERENCES

[1] S.-J. Chang and B.-C. Yu, "Mitochondrial matters of the brain: Mitochondrial dysfunction and oxidative status in epilepsy," *J. Bioenergetics Biomembranes*, vol. 42, no. 6, pp. 457–459, Dec. 2010.

[2] S. D. Shorvon, "The causes of epilepsy: Changing concepts of etiology of epilepsy over the past 150 years," *Epilepsia*, vol. 52, no. 6, pp. 1033–1044, Jun. 2011.

[3] M. Zhou, C. Tian, R. Cao, B. Wang, Y. Niu, T. Hu, H. Guo, and J. Xiang, "Epileptic seizure detection based on EEG signals and CNN," *Frontiers Neuroinform.*, vol. 12, p. 95, Dec. 2018.

[4] N. Nakasatp, M. F. Levesque, D. S. Barth, C. Baumgartner, R. L. Rogers, and W. W. Sutherling, "Comparisons of MEG, EEG, and ECoG source localization in neocortical partial epilepsy in humans," *Electroencephalogr. Clin. Neurophysiol.*, vol. 91, no. 3, pp. 171–178, Sep. 1994.

[5] O. David, T. Blauwblomme, A.-S. Job, S. Chabardès, D. Hoffmann, L. Minotti, and P. Kahane, "Imaging the seizure onset zone with stereo-electroencephalography," *Brain*, vol. 134, no. 10, pp. 2898–2911, Oct. 2011.

[6] C. C. Jouny, P. J. Franaszczuk, and G. K. Bergey, "Improving early seizure detection," *Epilepsy Behav.*, vol. 22, pp. S44–S48, Dec. 2011.

[7] M. K. Siddiqui, R. Morales-Menendez, X. Huang, and N. Hussain, "A review of epileptic seizure detection using machine learning classifiers," *Brain Informat.*, vol. 7, no. 1, pp. 1–18, Dec. 2020.

[8] K. Schindler, H. Leung, C. E. Elger, and K. Lehnertz, "Assessing seizure dynamics by analysing the correlation structure of multichannel intracranial EEG," *Brain*, vol. 130, no. 1, pp. 65–77, Nov. 2006.

[9] A. Puce and M. Hämäläinen, "A review of issues related to data acquisition and analysis in EEG/MEG studies," *Brain Sci.*, vol. 7, no. 12, p. 58, May 2017.

[10] E. J. Ngamga, S. Bialonski, N. Marwan, J. Kurths, C. Geier, and K. Lehnertz, "Evaluation of selected recurrence measures in discriminating pre-ictal and inter-ictal periods from epileptic EEG data," *Phys. Lett. A*, vol. 380, no. 16, pp. 1419–1425, Apr. 2016.

[11] D. A. Dean, A. L. Goldberger, R. Mueller, M. Kim, M. Rueschman, D. Mobley, S. S. Sahoo, C. P. Jayapandian, L. Cui, M. G. Morrical, S. Surovec, G.-Q. Zhang, and S. Redline, "Scaling up scientific discovery in sleep medicine: The national sleep research resource," *Sleep*, vol. 39, no. 5, pp. 1151–1164, May 2016.

[12] F. Tadel, S. Baillet, J. C. Mosher, D. Pantazis, and R. M. Leahy, "Brainstorm: A user-friendly application for MEG/EEG analysis," *Comput. Intell. Neurosci.*, vol. 2011, pp. 1–13, Oct. 2011.

[13] A. Gramfort, M. Luessi, E. Larson, D. A. Engemann, D. Strohmeier, C. Brodbeck, L. Parkkonen, and M. S. Hämäläinen, "MNE software for processing MEG and EEG data," *NeuroImage*, vol. 86, pp. 446–460, Feb. 2014.

[14] G. Li, S. Jiang, S. E. Paraskevopoulou, M. Wang, Y. Xu, Z. Wu, L. Chen, D. Zhang, and G. Schalk, "Optimal referencing for stereo-electroencephalographic (SEEG) recordings," *NeuroImage*, vol. 183, pp. 327–335, Dec. 2018.

[15] B. Boashash, M. Mesbah, and P. Colditz, "Newborn EEG seizure pattern characterisation using time-frequency analysis," in *Proc. IEEE Int. Conf. Acoust., Speech, Signal Process.*, vol. 2, May 2001, pp. 1041–1044.

[16] S. J. Schiff, T. Sauer, R. Kumar, and S. L. Weinstein, "Neuronal spatiotemporal pattern discrimination: The dynamical evolution of seizures," *NeuroImage*, vol. 28, no. 4, pp. 1043–1055, Dec. 2005.

[17] V. L. Dorr, M. Caparos, F. Wendling, J.-P. Vignal, and D. Wolf, "Extraction of reproducible seizure patterns based on EEG scalp correlations," *Biomed. Signal Process. Control*, vol. 2, no. 3, pp. 154–162, Jul. 2007.

[18] M. Fan and C.-A. Chou, "Detecting abnormal pattern of epileptic seizures via temporal synchronization of EEG signals," *IEEE Trans. Biomed. Eng.*, vol. 66, no. 3, pp. 601–608, Mar. 2019.

[19] X. Yao, X. Li, Q. Ye, Y. Huang, Q. Cheng, and G.-Q. Zhang, "A robust deep learning approach for automatic classification of seizures against non-seizures," 2018, *arXiv:1812.06562*. [Online]. Available: http://arxiv.org/abs/1812.06562

[20] S. Abramovici, A. Antony, M. E. Baldwin, A. Urban, G. Ghearing, J. Pan, T. Sun, R. T. Krafty, R. M. Richardson, and A. Bagic, "Features of simultaneous scalp and intracranial EEG that predict localization of ictal onset zone," *Clin. EEG Neurosci.*, vol. 49, no. 3, pp. 206–212, May 2018.

[21] W.-C. Chang, J. Kudlacek, J. Hlinka, J. Chvojka, M. Hadrava, V. Kumpost, A. D. Powell, R. Janca, M. I. Maturana, P. J. Karoly, D. R. Freestone, M. J. Cook, M. Palus, J. Otahal, J. G. R. Jefferys, and P. Jiruska, "Loss of neuronal network resilience precedes seizures and determines the ictogenic nature of interictal synaptic perturbations," *Nature Neurosci.*, vol. 21, no. 12, pp. 1742–1752, Dec. 2018.

[22] N. D. Truong, A. D. Nguyen, L. Kuhlmann, M. R. Bonyadi, J. Yang, S. Ippolito, and O. Kavehei, "Convolutional neural networks for seizure prediction using intracranial and scalp electroencephalogram," *Neural Netw.*, vol. 105, pp. 104–111, Sep. 2018.

[23] A. Sharma, J. K. Rai, and R. P. Tewari, "Scalp electroencephalography (sEEG) based advanced prediction of epileptic seizure time and identification of epileptogenic region," *Biomed. Eng./Biomedizinische Technik*, vol. 65, no. 6, pp. 705–720, Nov. 2020.

[24] Z. Zhang and K. K. Parhi, "Low-complexity seizure prediction from iEEG/sEEG using spectral power and ratios of spectral power," *IEEE Trans. Biomed. Circuits Syst.*, vol. 10, no. 3, pp. 693–706, Jun. 2016.

[25] A. S. Razavian, H. Azizpour, J. Sullivan, and S. Carlsson, "CNN features off-the-shelf: An astounding baseline for recognition," in *Proc. IEEE Conf. Comput. Vis. Pattern Recognit. Workshops*, Jun. 2014, pp. 806–813.

[26] Q. Wang, B. Li, T. Xiao, J. Zhu, C. Li, D. F. Wong, and L. S. Chao, "Learning deep transformer models for machine translation," 2019, *arXiv:1906.01787*. [Online]. Available: http://arxiv.org/abs/1906.01787

[27] G. Liu and J. Guo, "Bidirectional LSTM with attention mechanism and convolutional layer for text classification," *Neurocomputing*, vol. 337, pp. 325–338, Apr. 2019.

[28] A. I. Bandos, H. E. Rockette, T. Song, and D. Gur, "Area under the free-response ROC curve (FROC) and a related summary index," *Biometrics*, vol. 65, no. 1, pp. 247–256, Mar. 2009.

[29] P. Agarwal, H.-C. Wang, and K. Srinivasan, "Epileptic seizure prediction over eeg data using hybrid CNN-SVM model with edge computing services," in *Proc. MATEC Web Conf.*, vol. 210, 2018, p. 03016.

[30] Y. Qian and P. C. Woodland, "Very deep convolutional neural networks for robust speech recognition," in *Proc. IEEE Spoken Lang. Technol. Workshop (SLT)*, Dec. 2016, pp. 481–488.

[31] Y. Zhan, M. I. Vai, S. Barma, S. H. Pun, J. W. Li, and P. U. Mak, "A computation resource friendly convolutional neural network engine for EEG-based emotion recognition," in *Proc. IEEE Int. Conf. Comput. Intell. Virtual Environ. Meas. Syst. Appl. (CIVEMSA)*, Jun. 2019, pp. 1–6.

[32] X. Zhang, L. Yao, M. Dong, Z. Liu, Y. Zhang, and Y. Li, "Adversarial representation learning for robust patient-independent epileptic seizure detection," *IEEE J. Biomed. Health Informat.*, vol. 24, no. 10, pp. 2852–2859, Oct. 2020.
[33] S. Alhagry, A. Aly, and R. A. El-Khoribi, "Emotion recognition based on EEG using LSTM recurrent neural network," *Int. J. Adv. Comput. Sci. Appl.*, vol. 8, no. 10, pp. 355–358, 2017.
[34] G. Krishna, C. Tran, M. Carnahan, and A. H. Tewfik, "EEG based continuous speech recognition using transformers," 2019, *arXiv:2001.00501*. [Online]. Available: http://arxiv.org/abs/2001.00501
[35] A. Vaswani, N. Shazeer, N. Parmar, J. Uszkoreit, L. Jones, A. N. Gomez, L. Kaiser, and I. Polosukhin, "Attention is all you need," 2017, *arXiv:1706.03762*. [Online]. Available: http://arxiv.org/abs/1706.03762

HAO YU was born in Hubei, China, in 1997. He received the B.S. degree in software engineering from the University of Shanghai for Science and Technology, Shanghai, China, in 2018. He is currently pursuing the master's degree in software engineering from East China Normal University. Since 2018, he has been engaged in research on brain signal processing and analysis, data mining, and machine learning.

MENGQI HU was born in Shanghai, China, in 1997. He received the B.S. degree in software engineering from East China Normal University, Shanghai, in 2020, where he is currently pursuing the M.S. degree in software engineering. Since 2018, he has been engaged in research on brain signal processing, data mining, and deep learning.